

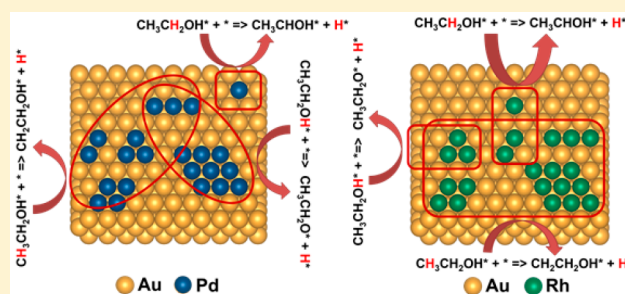
Dehydrogenation Selectivity of Ethanol on Close-Packed Transition Metal Surfaces: A Computational Study of Monometallic, Pd/Au, and Rh/Au Catalysts

Hao Li and Graeme Henkelman*

Department of Chemistry and the Institute for Computational Engineering and Sciences, The University of Texas at Austin, 1 University Station A5300, Austin, Texas 78712-0165, United States

S Supporting Information

ABSTRACT: Ethanol (EtOH) decomposition has been widely studied in recent years. However, the initial dehydrogenation selectivity on catalytic surfaces, which plays a crucial role in EtOH partial oxidation and steam reforming, is not well understood. Here, density functional theory (DFT) was used to calculate the initial dehydrogenation selectivities of EtOH on monometallic and X/Au (X = Pd and Rh) close-packed surfaces. The energy for the initial bond scissions of O–H and α - and β -C–H were calculated on each surface. The binding energy of EtOH is found to be a good reactivity descriptor for the scission of O–H and β -C–H bonds, while the binding energy of CH_3CHOH is a good reaction descriptor for α -C–H bond scission. The scaling relationships between the activation energy barriers and binding energies on Pd/Au and Rh/Au surface alloys are significantly different from those of monometallic surfaces. Additionally, the specific atomic ensembles on the Pd/Au and Rh/Au surfaces have different initial dehydrogenation selectivities of EtOH. Our calculated scaling relationships were used to construct contour plots that provide predictive trends for the selectivity of the initial EtOH dehydrogenation. We conclude that the presence of specific atomic ensembles on the surface of alloy catalysts can efficiently control the reaction products of EtOH dehydrogenation.



1. INTRODUCTION

Ethanol (EtOH) is a versatile hydrogen source that can be produced from biomass carbohydrate fermentation.¹ Many industrially significant chemical processes, such as steam reforming and production of acetaldehyde, acetic acid, and ethyl esters, involve the decomposition of EtOH on catalytic surfaces.^{2–5} For the decomposition of EtOH, bond scission of O–H (R1) or α/β -C–H (R2 and R3, respectively) is the initial step before bond scission of C–O and C–C.^{4–8} The initial dehydrogenation selectivity of EtOH can directly determine the primary reaction pathway and the selectivity of products,⁴ such as EtOH selective oxidation.^{9,10} Formation of acetaldehyde is considered a crucial initial step leading to subsequent oxidation reactions so that understanding selectivity of the initial step of EtOH dehydrogenation is particularly important.

O–H bond scission:

 α -C–H bond scission: β -C–H bond scission:

Previous studies, both theoretical^{6–8,10,11} and experimental,^{4,5,9} have shown that the selectivity of the initial dehydrogenation step of EtOH varies for different monometallic close-packed transition metal surfaces. On alloyed surfaces, experimental studies show that specific compositions of bimetallics are able to perform selective H_2 conversion from EtOH,¹² which then affects the subsequent sequence of dehydrogenation reactions. However, the microscopic details of the selectivity of bond breaking on alloy surfaces is hard to determine experimentally because alloyed surfaces typically contain a distribution of atomic ensembles (specific arrangements of group of atoms),^{13–18} leading to a distribution of activities at different locations on the surface.

Fortunately, atomic ensemble effects on alloy systems can be studied using density functional theory (DFT), which is a powerful tool that can provide an understanding of the activity of alloyed surface at the microscopic scale. Previous studies have shown that different atomic ensembles on Pd/Au¹⁹ and Pt/Au²⁰ have specific decomposition selectivities of formic acid, leading to different pathways and products of the overall reaction. Experiments also show that formic acid decomposition on Pd/Au systems are quite different from that of pure

Received: October 8, 2017

Revised: November 15, 2017

Published: November 20, 2017

Pd.²¹ More recently, we discovered that the dehydrogenation of EtOH on Pd–Au model catalysts with varying Pd content can lead to different H₂ production selectivities and activities, with the bifunctional effect that Pd(111)-like ensembles are favorable for EtOH dehydrogenation while the Pd–Au interface ensembles are more favorable for H₂ association.²² Other theoretical studies provide additional mechanistic insights on alcohol dehydrogenation, including EtOH oxidation on Pt₃M (M = Pt, Ru, Sn, Re, Rh and Pd) catalysts^{23–25} and methanol dehydrogenation on the Pd–Zn surface alloy.²⁶ However, to the best of our knowledge, few previous studies have specifically focused on the atomic ensemble effects for EtOH dehydrogenation.

To study the initial dehydrogenation selectivity of EtOH, the DFT-calculated activation energy barrier (E_{act}) is an important indicator for comparing reaction rates. To reduce the computational cost, Brønsted–Evans–Polanyi (BEP) relationships are widely used to describe correlations between E_{act} and reaction energies.²⁷ Fajín et al. reported that a generalized BEP relationship can be applied to estimate the E_{act} of O–H bond cleavage of organic molecules and water on various transition metal surfaces.²⁸ However, for EtOH, the initial bond scission of O–H might not always be the most favorable step on many metallic systems and descriptors that describe the three initial dehydrogenation selectivities (R1–R3) are not well understood.

In this work, the initial dehydrogenation step of EtOH is calculated on the close-packed surfaces of both mono and bimetallic catalysts. Then, in order to have a more general model of activity, we use a simplified descriptor, the binding energy (E_b) of the reaction species, which is correlated with the E_{act} of the initial dehydrogenation steps through a BEP relationship. The binding energy of EtOH ($E_b[\text{EtOH}]$) was found to be a good descriptor for the –H bond scission of end groups (O–H and β -C–H), while the binding energy of CH₃CHOH ($E_b[\text{CH}_3\text{CHOH}]$) was found to be a good descriptor for α -C–H bond scission. As well as monometallic surfaces, two alloy surfaces X/Au (X = Pd and Rh) with varying X ensemble sizes were studied. The choice of Pd/Au and Rh/Au was motivated by the observation that they represent two types of miscibilities: Pd/Au is classically miscible, and the alloy should have many Pd/Au interface sites;²¹ while Rh/Au is classically immiscible it has been recently synthesized by advanced techniques (e.g., microwave-assisted synthesis^{18,29})—it should have a greater fraction of pure monometallic regions separated by Rh/Au interface sites on the surface. Thus, Pd/Au and Rh/Au are expected have different dominant ensembles on their surfaces with Pd/Au having more alloyed atomic ensembles and Rh/Au having more monometallic ensembles. For the alloys discussed here, we have selected a set of typical ensembles that include both alloyed and monometallic ensembles.

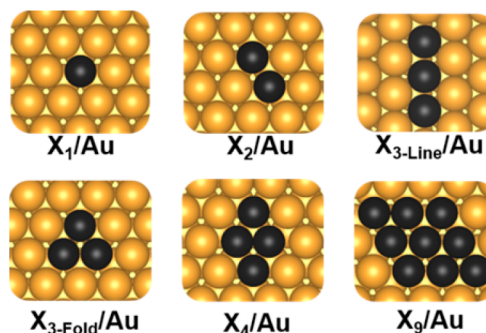
2. COMPUTATIONAL MODELS AND METHODS

DFT calculations were conducted with the Vienna *ab initio* simulation package (VASP). Core electrons were described via the projector augmented-wave method.^{30,31} The generalized gradient approximation with the Perdew–Burke–Ernzerhof (PBE) functional was used to describe electronic exchange and correlation.³² Soft potentials were used to describe oxygen and carbon. Kohn–Sham wave functions were expanded in a plane wave basis for the valence electrons³³ with an energy cutoff of 300 eV. van der Waals corrections (DFT-D3) were used for the

calculations of binding energies.³⁴ The Brillouin zone was sampled with a $3 \times 3 \times 1$ Monkhorst–Pack k -point mesh.³⁵ All E_{act} were calculated with the climbing image nudged elastic band (cNEB) method.³⁶ For each surface, multiple reaction pathways were found and those with the lowest E_{act} were determined. Geometries were considered optimized when the force on each atom was less than 0.05 eV/Å. Spin polarization was used for calculations on Ni and Co surfaces, and for the total energies of CH₃CH₂O, CH₃CHOH and CH₂CH₂OH. Convergence of our calculations was tested by increasing the energy cutoff to 400 eV using the standard PAW potentials; all tested binding energies (EtOH, EtOH reaction species and H) on Pd(111), Rh(111), and Au(111) were found to vary by no more than 0.03 eV. No significant change was found in the relaxed configurations. Similar tests for the cNEB calculations on Pd(111), Rh(111), and Au(111) show that differences of E_{act} are at most 0.05 eV for the dehydrogenation selectivities (R1–R3).

All calculations were modeled on 4-layer, (4 × 4) unit cell, close-packed surfaces. For Au, Ag, Cu, Pd, Rh, Ni, Pt, and Ir and all X/Au (X = Pd and Rh) surface alloys, reactions were considered on the (111) surface. For Ru and Co the (0001) surface was chosen. For the X/Au (X = Pd and Rh) surface alloys, the first layer consisted of the X/Au surface alloys with varying X ensemble sizes (Scheme 1), while the bottom three

Scheme 1. Surfaces of X/Au (X = Pd and Rh) Considered^a



^aBlack spheres represent X atoms (X = Pd and Rh); yellow spheres are Au.

layers were pure Au (Scheme 1). The bottom two layers of the slabs were kept fixed in bulk positions and the top two layers were allowed to relax. The most favorable binding configuration of EtOH on the surfaces was found to be a “laying-down” configuration,³⁷ with O bonding to the atop site and C–C bond being parallel to the surfaces. All binding energies E_b (except for H) were calculated using

$$E_b = E_{slab+molecule} - E_{slab} - E_{molecule} \quad (1)$$

where $E_{slab+molecule}$ is the total energy of the slab with one adsorbed molecule, E_{slab} is the total energy of the bare slab, and $E_{molecule}$ is the energy of the molecule in vacuum. The H binding energies E_H were calculated using

$$E_H = E_{slab+H} - E_{slab} - \frac{1}{2}E_{H_2} \quad (2)$$

where E_{slab+H} is the total energy of the slab with one adsorbed H, and E_{H_2} is the energy of a H₂ molecule in vacuum.

3. RESULTS AND DISCUSSION

3.1. Scaling Relationships and Descriptors. To study trends of the initial dehydrogenation steps of EtOH on different surfaces, we start by looking for scaling relationships between E_{act} and the binding energy, E_b , of the reaction species, as identified in R1–R3. Parts a and c of Figure 1 show that for R1 and R3, E_{act} correlates well with $E_b[\text{EtOH}]$. For R2, E_{act} correlates much better with $E_b[\text{CH}_3\text{CHOH}]$ (Figure 1b), than those with $E_b[\text{EtOH}]$ (Figure S1). Therefore, we conclude that for EtOH dehydrogenation, $E_b[\text{EtOH}]$ is a good descriptor for R1 and R3, while $E_b[\text{CH}_3\text{CHOH}]$ is a good descriptor for R2. Interestingly, for R1 and R3, trends of X/Au (X = Pd and Rh) surface alloys are significantly different from those developed from monometallic surfaces. For R2, although most of the points calculated on alloys are consistent with the trend of monometallics, the trends of Pd/Au and Rh/Au are also somewhat different from that of monometallics. These differences likely originate from the uneven redistribution of electrons upon alloying, leading to different chemical properties as compared with the monometallic surfaces. It should be noted that Pd/Au has very different trends from Rh/Au, which indicates that the relationships are sensitive to the specific component metals. Therefore, the relationships developed from monometallic surfaces are not representative of alloy surfaces, and for each specific alloy, separate correlations should be determined. From these relationships we can see that E_{act} generally decreases as the binding of EtOH or CH_3CHOH increases, indicating that strengthening the binding energy of reaction species facilitates dehydrogenation. Interestingly, this result is somewhat different from conclusions drawn from previous volcano activity plots, which suggest that an optimal reaction activity will be reached if the adsorbate binding is neither too strong nor too weak, such as $\text{C}=\text{C}$ hydrogenation reactions in our previous studies.^{14,15,17} However, EtOH dehydrogenation is a special case in that stronger adsorbate binding leads to a stronger driving force to break the O–H and C–H bonds, leading to a lower activation barrier.

3.2. Initial Dehydrogenation Selectivity on X/Au (X = Pd and Rh). It is generally understood that atomic ensemble effects are the primary feature that determines the local reactivity on alloy catalysts,^{13–15,17,18} and that electronic and strain effects are less important which both component metals are present on the surface. For EtOH oxidation on Pt-based bimetallics, a generally accepted explanation is the bifunctional mechanism, where Pt sites are favorable for EtOH dissociative adsorption while the other metal is favorable for water dissociation.³⁸ This mechanism also suggests that specific ensemble arrangement on alloyed surface could promote EtOH-related reactions. To discuss the atomic ensemble effects more clearly, plotting the dehydrogenation barriers as a function of ensemble size is an intuitive way to see how atomic ensembles affect the initial dehydrogenation selectivity on alloys. Figure 2 shows that for Pd/Au, with the exception of Pd_{3-Line}/Au, the E_{act} of R1–R3 on Pd_x/Au surface alloys decrease monotonically with increasing Pd ensemble size x from 1 to 9 (Figure 2a). For the Pd_{3-Line}/Au ensemble, scission of O–H and β -C–H compete with each other. Compared to Pd/Au, the trends of E_{act} on Rh/Au are less predictable: though the E_{act} of β -C–H bond scission generally decreases monotonically, the E_{act} of O–H and α -C–H bond scissions (R1 and R2, respectively) fluctuate with the Rh ensemble sizes. Even though the trends on Rh/Au are not monotonic, most of the calculated

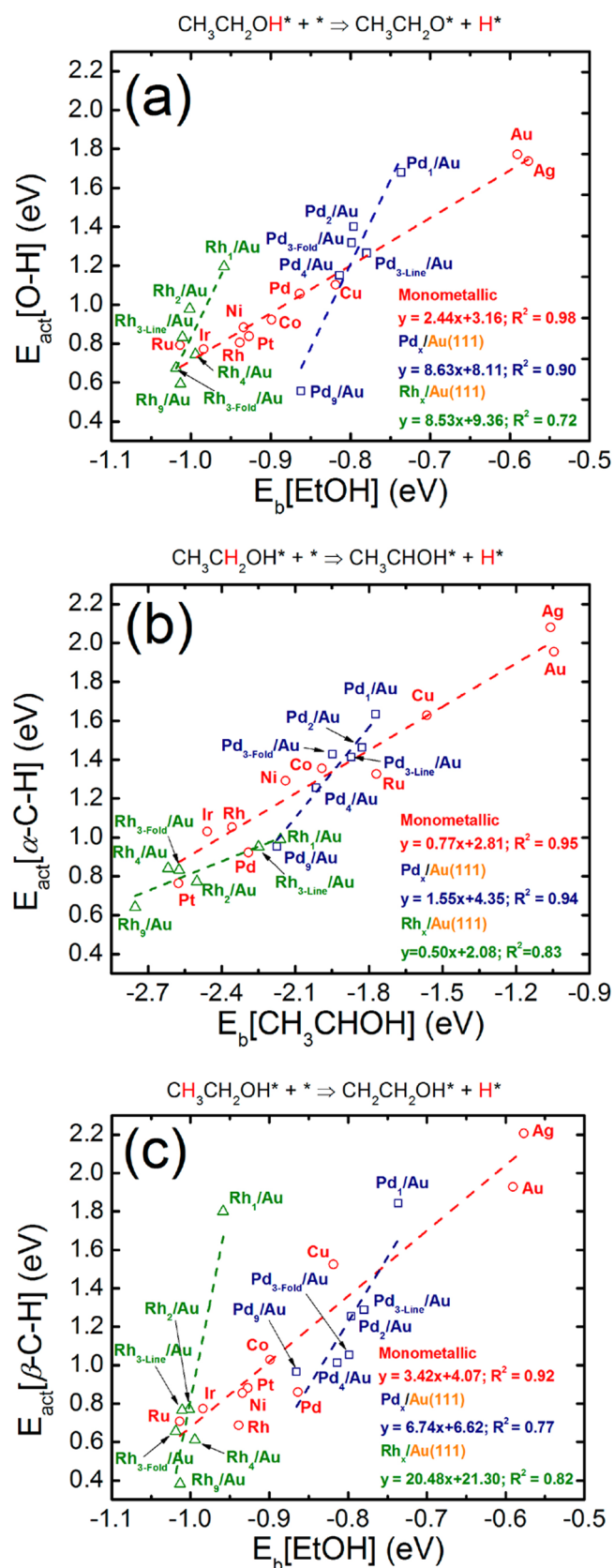


Figure 1. Correlation of (a) $E_{act}[\text{O-H}]$ vs $E_b[\text{EtOH}]$, (b) $E_{act}[\alpha\text{-C-H}]$ vs $E_b[\text{CH}_3\text{CHOH}]$ and (c) $E_{act}[\beta\text{-C-H}]$ vs $E_b[\text{EtOH}]$. Red lines and dots represent the trends of monometallic surfaces, blue is for Pd/Au, and green is for Rh/Au. The E_b and E_{act} data are given in Table S1.

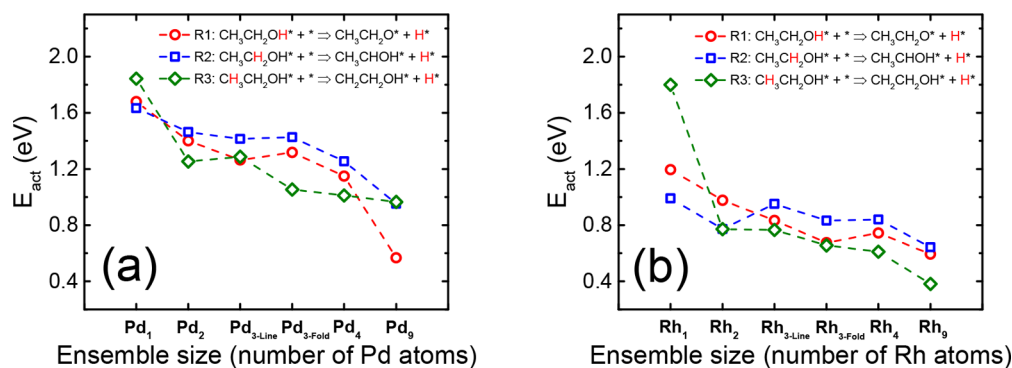
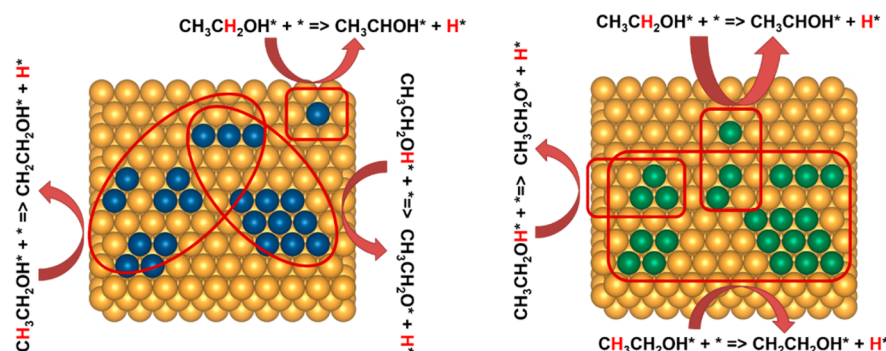


Figure 2. Initial EtOH dehydrogenation barriers as a function of ensemble size on (a) Pd/Au and (b) Rh/Au surface alloys. Schematic illustration of ensembles considered for these calculations are shown in Scheme 1; the initial and final states of the reactions are shown in Figure S2.

Scheme 2. Schematic Illustration of the Favorable Initial EtOH Dehydrogenation Mechanism on Different Pd/Au and Rh/Au Ensembles^a



^aYellow spheres represent Au atoms, blue represent Pd, and green represent Rh.

Rh/Au surfaces are more favorable for β -C–H bond scissions (R3) during the initial dehydrogenation. Exceptions to the selective β -C–H bond scission are Rh₁/Au, Rh₂/Au and Rh_{3-Fold}/Au: Rh₁/Au is more favorable for α -C–H bond scissions (R1); Rh₂/Au is favorable for bond scissions of both α - and β -C–H (R2 and R3, respectively); Rh_{3-Fold}/Au is favorable for bond scissions of both O–H and β -C–H (R1 and R3). Schematic illustrations of the selectivities on both Pd/Au and Rh/Au surface alloys are shown in Scheme 2.

Interestingly, both Pd₁/Au and Rh₁/Au are selective to R2, which is the step not usually favored on monometallic surfaces.⁴ A reason for this special selectivity is that Au binds to carbon species more weakly than Pd and Rh. For X₁/Au (X = Pd or Rh) surfaces, bond scission of β -C–H leads to a final state in which the β -carbon binds to the adjacent Au atop site, rather than the Pd or Rh atop site (Figure S2). Thus, the single-atom alloy surfaces are less likely to break the β -C–H bond. We also expect that other X₁/Au single atom alloys (where X is a strong carbon-binding metal, such as Pt or Ir) will have a similar selectivity.

As the composition of the X/Au (X = Pd and Rh) alloys are varied, different atomic ensembles will be dominant on the surface, which can in turn change the favorable initial dehydrogenation mechanism. The calculations show that pure Au has very high E_{act} in each of R1–R3 (Figure 1), so that pure Au ensembles are catalytically inactive, which is consistent with our recent experimental results.²² On the other hand, if the X composition is low, the presence of single-atom surface alloys can lead to selective scission of the α -C–H bond (R2). Particularly for Pd/Au, which is a classically miscible alloy,

small Pd ensembles should be ubiquitous if the Pd composition is not too high, leading to scissions of both α - and β -C–H (R2 and R3). If the structure of Pd/Au is core@shell or partial core@shell, selective scission of O–H (R1) should be favorable, since it is analogous to the Pd₉/Au surface considered in our calculations. Rh/Au, on the other hand, is a classically immiscible alloy,^{39,40} so that at least thermodynamically, some surface segregation should lead to the formation of large monometallic Rh and Au ensembles. Therefore, when the Rh composition is sufficiently high, pure Rh ensembles will result in similar dehydrogenation mechanisms as calculated on Rh₄/Au and Rh₉/Au where β -C–H bond scission is dominant.

The alloying effect on EtOH dehydrogenation can be understood from the calculated H binding energies (Figure S3). For both Pd/Au and Rh/Au, the H binding energy changes significantly when the number of Pd or Rh in the ensemble increases from one to three but when the alloy element cluster is larger than three, the H binding energy tends to plateau. The Pd/Au and Rh/Au alloy surfaces with large X ensembles (X = Pd and Rh) contain both monometallic X(111)-like sites and bimetallic X–Au interface sites. The alloy interface sites have significantly different EtOH dehydrogenation properties as compared to the monometallic sites.²² Using ultrahigh vacuum (UHV) experiments and DFT calculations, our recent study has shown that different compositions of Pd(111)-like sites and Pd–Au interface sites on the catalytic surface lead to different EtOH dehydrogenation mechanisms.²² Similar conclusions were drawn for formic acid dehydrogenation on Pd/Au.^{19,21}

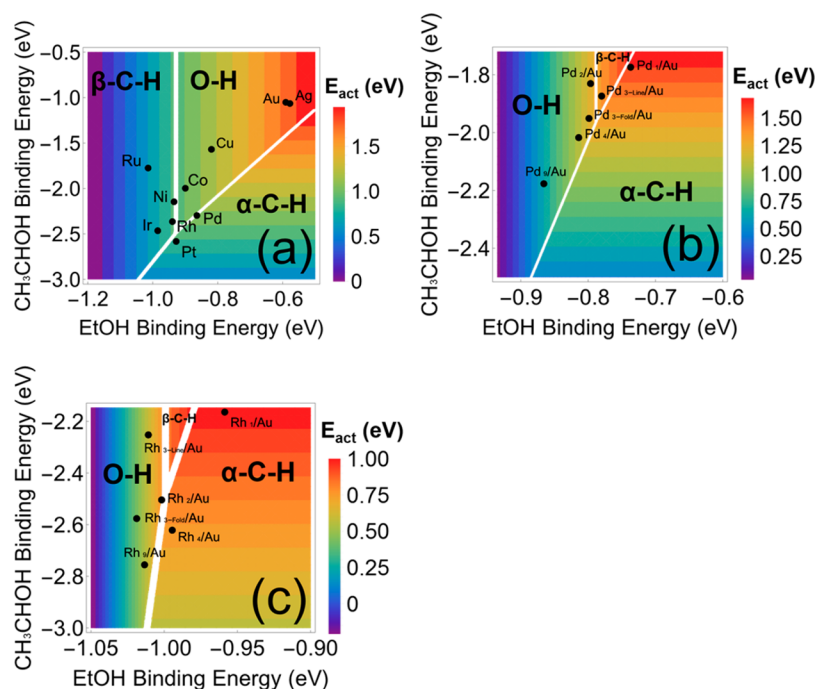


Figure 3. Contour plots of the initial dehydrogenation selectivities of EtOH on (a) monometallic, (b) Pd/Au, and (c) Rh/Au surfaces.

The electronic structure of the alloy ensembles can also help with understanding their reactivity. Here, we calculated the projected density of states (PDOS) of the d-band of the triatomic ensemble, which is the smallest surface unit that provides the 3-fold hollow site for H adsorption (Figure S4). If the number of Pd or Rh is low (ensembles of X₁, X₂ and X_{3-Line}), the triatomic ensembles have less contracted PDOS distributions than those surfaces with more alloyed Pd or Rh. With more alloyed Pd or Rh, the d-band is closer to the Fermi level, indicating stronger binding to EtOH-related species and a higher activity to redox reduction such as EtOH decomposition.¹¹

3.3. Selectivity Plots. With calculated scaling relationships between E_{act} and E_b (Figure 1), general trends for the selectivity of R1–R3 can be determined. Following the hypothesis that the reaction with the lowest E_{act} (among R1–R3) has the most favorable reaction selectivity, contour plots can be generated as

$$E_{act}[\text{Min}] = \text{Min}\{E_{act}[\text{O} - \text{H}], E_{act}[\alpha - \text{C} - \text{H}], E_{act}[\beta - \text{C} - \text{H}]\} \quad (3)$$

where $E_{act}[\text{Min}]$ is the lowest E_{act} among the three dehydrogenation reaction mechanisms, where $E_{act}[\text{O} - \text{H}]$, $E_{act}[\alpha - \text{C} - \text{H}]$, and $E_{act}[\beta - \text{C} - \text{H}]$ are expressed through the scaling relations shown in Figure 1.

With the result from section 3.1 that E_{act} scales with $E_b[\text{EtOH}]$ for R1 and R3, and with $E_b[\text{CH}_3\text{CHOH}]$ for R2, the contour plots for the R1–R3 selectivities can be generated as a functions of these two descriptors. Figure 3 is a selectivity contour plot that is divided into three zones, favoring O–H, α–C–H and β–C–H bond breaking, which correspond to selectivity for R1–R3, respectively. Figure 3a shows that for Au, Ag, Cu, and Co, scission of O–H (R1) is dominant. For other monometallics, more than one reaction compete since they are close to the boundary between two pathways: for Ni and Rh, bond scissions of O–H (R1) and β–C–H (R3) are comparable; for Pd, bond scissions of O–H (R1) and α–C–H

(R2) are comparable. The selectivity contours for Pd/Au and Rh/Au as a function of $E_b[\text{EtOH}]$ and $E_b[\text{CH}_3\text{CHOH}]$ are different from those of the monometallic surfaces (Figure 3, parts b and c). The alloy contour plots indicate that atomic ensembles on X/Au (X = Pd or Rh) significantly influence the initial dehydrogenation selectivity. It should be noted that such contour plots are dependent on the specific alloy, since the scaling relation between E_{act} and E_b are element specific. In fact, one of our results is that due to the synergetic influences of the atomic ensemble and electronic effects, different alloys will have different selectivity trends as a function of composition.

4. CONCLUSION

In this paper, we have calculated trends for the initial dehydrogenation selectivity of EtOH on monometallic and X/Au (X = Pd and Rh) close-packed surfaces. We find that the scaling relationships of E_{act} versus binding energies on X/Au (X = Pd and Rh) surface alloys are different from those of monometallic surfaces. $E_b[\text{EtOH}]$ is found to be good reaction descriptor for R1 and R3, whereas $E_b[\text{CH}_3\text{CHOH}]$ is a good reaction descriptor for R2. We show that the initial dehydrogenation selectivities of EtOH on X/Au (X = Pd and Rh) surface alloys are dependent primarily on the atomic ensemble size, and to some extent shape. We also found that Pd₁/Au and Rh₁/Au (single-atom alloys) are highly selective for R2, which is the step that is seldom active on monometallic surfaces. Finally, predictive models for the initial dehydrogenation of EtOH were calculated in the form of selectivity contour plots as functions of $E_b[\text{EtOH}]$ and $E_b[\text{CH}_3\text{CHOH}]$. With these, synthesis of specific atomic ensembles can be targeted to control the selectivity of EtOH dehydrogenation and subsequent reactions such as EtOH oxidation and decomposition.

■ ASSOCIATED CONTENT

Supporting Information

The material is available free of charge via the Internet at The Supporting Information is available free of charge on the ACS Publications website at DOI: 10.1021/acs.jpcc.7b09953.

Data of binding energies and activation energy barriers, regression relationships between the α -C–H bond scission barrier and EtOH binding energy, schematic illustrations of the catalytic surfaces and initial and final states for the cNEB calculations, H binding energies on alloy surfaces, and PDOS of the d-band of alloyed triatomic ensembles (PDF)

■ AUTHOR INFORMATION

Corresponding Author

*E-mail: henkelman@utexas.edu (G.H.).

ORCID

Graeme Henkelman: 0000-0002-0336-7153

Notes

The authors declare no competing financial interest.

■ ACKNOWLEDGMENTS

This work was supported by the National Science Foundation (CHE-1534177) the Department of Energy, Basic Energy Sciences (DE-SC0010576), and the Welch Foundation (F-1841). Computational resources were provided by the Texas Advanced Computing Center and the National Energy Research Scientific Computing Center.

■ REFERENCES

- (1) Lin, Y.; Tanaka, S. Ethanol Fermentation from Biomass Resources: Current State and Prospects. *Appl. Microbiol. Biotechnol.* **2006**, *69*, 627–642.
- (2) Klouze, V.; Fierro, V.; Denton, P.; Katz, H.; Lisse, J. P.; Bouvot-Mauduit, S.; Mirodatos, C. Ethanol Reforming for Hydrogen Production in a Hybrid Electric Vehicle: Process Optimisation. *J. Power Sources* **2002**, *105*, 26–34.
- (3) Rass-Hansen, J.; Falsig, H.; Jørgensen, B.; Christensen, C. H. Bioethanol: Fuel or Feedstock? *J. Chem. Technol. Biotechnol.* **2007**, *82*, 329–333.
- (4) Zanchet, D.; Santos, J. B. O.; Damyanova, S.; Gallo, J. M. R.; Bueno, J. M. C. Toward Understanding Metal-Catalyzed Ethanol Reforming. *ACS Catal.* **2015**, *5*, 3841–3863.
- (5) Williams, R. M.; Pang, S. H.; Medlin, J. W. O-H versus C-H Bond Scission Sequence in Ethanol Decomposition on Pd(111). *Surf. Sci.* **2014**, *619*, 114–118.
- (6) Li, M.; Guo, W.; Jiang, R.; Zhao, L.; Shan, H. Decomposition of Ethanol on Pd(111): A Density Functional Theory Study. *Langmuir* **2010**, *26*, 1879–1888.
- (7) Choi, Y.; Liu, P. Understanding of Ethanol Decomposition on Rh(111) from Density Functional Theory and Kinetic Monte Carlo Simulations. *Catal. Today* **2011**, *165*, 64–70.
- (8) Zhang, J.; Cao, X. M.; Hu, P.; Zhong, Z.; Borgna, A.; Wu, P. Density Functional Theory Studies of Ethanol Decomposition on Rh(211). *J. Phys. Chem. C* **2011**, *115*, 22429–22437.
- (9) Gong, J.; Mullins, C. B. Selective Oxidation of Ethanol to Acetaldehyde on Gold. *J. Am. Chem. Soc.* **2008**, *130*, 16458–16459.
- (10) Wang, H. F.; Liu, Z. P. Comprehensive Mechanism and Structure-Sensitivity of Ethanol Oxidation on Platinum: New Transition-State Searching Method for Resolving the Complex Reaction Network. *J. Am. Chem. Soc.* **2008**, *130*, 10996–11004.
- (11) Wang, J. H.; Lee, C. S.; Lin, M. C. Mechanism of Ethanol Reforming: Theoretical Foundations. *J. Phys. Chem. C* **2009**, *113*, 6681–6688.

(12) Kumar, A.; Prasad, R.; Sharma, Y. C. Steam Reforming of Ethanol: Production of Renewable Hydrogen. *Int. J. Environ. Res. Dev.* **2014**, *4*, 2249–3131.

(13) Liu, P.; Nørskov, J. K. Ligand and Ensemble Effects in Adsorption on Alloy Surfaces. *Phys. Chem. Chem. Phys.* **2001**, *3*, 3814–3818.

(14) Kunal, P.; Li, H.; Dewing, B. L.; Zhang, L.; Jarvis, K.; Henkelman, G.; Humphrey, S. M. Microwave-Assisted Synthesis of Pd_xAu_{100-x} Alloy Nanoparticles: A Combined Experimental and Theoretical Assessment of Synthetic and Compositional Effects upon Catalytic Reactivity. *ACS Catal.* **2016**, *6*, 4882–4893.

(15) Luo, L.; Duan, Z.; Li, H.; Kim, J.; Henkelman, G.; Crooks, R. M. Tunability of the Adsorbate Binding on Bimetallic Alloy Nanoparticles for the Optimization of Catalytic Hydrogenation. *J. Am. Chem. Soc.* **2017**, *139*, 5538–5546.

(16) Seraj, S.; Kunal, P.; Li, H.; Henkelman, G.; Humphrey, S. M.; Werth, C. J. PdAu Alloy Nanoparticle Catalysts: Effective Candidates for Nitrite Reduction in Water. *ACS Catal.* **2017**, *7*, 3268–3276.

(17) Piburn, G. W.; Li, H.; Kunal, P.; Henkelman, G.; Humphrey, S. M. Rapid Synthesis of RhPd Alloy Nanocatalysts. *ChemCatChem* **2017**, DOI: 10.1002/cctc.201701133.

(18) García, S.; Zhang, L.; Piburn, G. W.; Henkelman, G.; Humphrey, S. M. Microwave Synthesis of Classically Immiscible Rhodium-Silver and Rhodium-Gold Alloy Nanoparticles: Highly Active Hydrogenation Catalysts. *ACS Nano* **2014**, *8*, 11512–11521.

(19) Yuan, D. W.; Liu, Z. R. Atomic Ensemble Effects on Formic Acid Oxidation on PdAu Electrode Studied by First-Principles Calculations. *J. Power Sources* **2013**, *224*, 241–249.

(20) Zhong, W.; Qi, Y.; Deng, M. The Ensemble Effect of Formic Acid Oxidation on Platinum-Gold Electrode Studied by First-Principles Calculations. *J. Power Sources* **2015**, *278*, 203–212.

(21) Yu, W. Y.; Mullen, G. M.; Flaherty, D. W.; Mullins, C. B. Selective Hydrogen Production from Formic Acid Decomposition on Pd-Au Bimetallic Surfaces. *J. Am. Chem. Soc.* **2014**, *136*, 11070–11078.

(22) Evans, E. J.; Li, H.; Yu, W.-Y.; Mullen, G. M.; Henkelman, G.; Mullins, C. B. Mechanistic Insights on Ethanol Dehydrogenation on Pd–Au Model Catalysts: A Combined Experimental and DFT Study. *Phys. Chem. Chem. Phys.* **2017**, *19*, 30578.

(23) Xu, Z. F.; Wang, Y. Effects of Alloyed Metal on the Catalysis Activity of Pt for Ethanol Partial Oxidation: Adsorption and Dehydrogenation on Pt₃M (M = Pt, Ru, Sn, Re, Rh, and Pd). *J. Phys. Chem. C* **2011**, *115*, 20565–20571.

(24) Xu, Z.; Wang, Y. Understanding Electrochemical Activity Enhancement of Bimetallic Particles to Ethanol Electro-Oxidation: Ethanol Adsorption and Decomposition on Pt_nM (n = 6 and 9; M = Pt, Ru, and Sn). *ACS Symp. Ser.* **2013**, *1133*, 135–151.

(25) Pérez, A. E.; Ribadeneira, R. Use of Chemical Descriptors Approach and DFT to Analyze the C–C Bond Cleavage on Pt₃Re₁ Alloy in the Ethanol Oxidation Reaction for Fuel Cells. *J. Electroanal. Chem.* **2017**, *791*, 185–195.

(26) Huang, Y.; Chen, Z. X. Density Functional Investigations of Methanol Dehydrogenation on Pd-Zn Surface Alloy. *Langmuir* **2010**, *26*, 10796–10802.

(27) Evans, M. G.; Polanyi, M. Inertia and Driving Force of Chemical Reactions. *Trans. Faraday Soc.* **1938**, *34*, 11.

(28) Fajín, J. L. C.; Cordeiro, M. N. D. S.; Illas, F.; Gomes, J. R. B. Generalized Brønsted-Evans-Polanyi Relationships and Descriptors for O–H Bond Cleavage of Organic Molecules on Transition Metal Surfaces. *J. Catal.* **2014**, *313*, 24–33.

(29) House, S. D.; Bonifacio, C. S.; Timoshenko, J.; Kunal, P.; Wan, H.; Duan, Z.; Li, H.; Yang, J. C.; Frenkel, A. I.; Humphrey, S. M.; et al. Computationally Assisted STEM and EXAFS Characterization of Tunable Rh/Au and Rh/Ag Bimetallic Nanoparticle Catalysts. *Microsc. Microanal.* **2017**, *23*, 2030–2031.

(30) Blöchl, P. E. Projector Augmented-Wave Method. *Phys. Rev. B: Condens. Matter Mater. Phys.* **1994**, *50*, 17953–17979.

(31) Kresse, G.; Furthmüller, J. Efficient Iterative Schemes for Ab Initio Total-Energy Calculations Using a Plane-Wave Basis Set. *Phys. Rev. B: Condens. Matter Mater. Phys.* **1996**, *54*, 11169–11186.

- (32) Perdew, J. P.; Burke, K.; Ernzerhof, M. Generalized Gradient Approximation Made Simple. *Phys. Rev. Lett.* **1996**, *77*, 3865–3868.
- (33) Kohn, W.; Sham, L. J. Self-Consistent Equations Including Exchange and Correlation Effects. *Phys. Rev.* **1965**, *140*, A1133.
- (34) Grimme, S.; Antony, J.; Ehrlich, S.; Krieg, H. A Consistent and Accurate Ab Initio Parametrization of Density Functional Dispersion Correction (DFT-D) for the 94 Elements H-Pu. *J. Chem. Phys.* **2010**, *132*, 154104.
- (35) Monkhorst, H.; Pack, J. Special Points for Brillouin Zone Integrations. *Phys. Rev. B* **1976**, *13*, 5188–5192.
- (36) Henkelman, G.; Uberuaga, B. P.; Jónsson, H. A Climbing Image Nudged Elastic Band Method for Finding Saddle Points and Minimum Energy Paths. *J. Chem. Phys.* **2000**, *113*, 9901–9904.
- (37) Tereshchuk, P.; Da Silva, J. L. F. Ethanol and Water Adsorption on Close-Packed 3d, 4d, and 5d Transition-Metal Surfaces: A Density Functional Theory Investigation with van Der Waals Correction. *J. Phys. Chem. C* **2012**, *116*, 24695–24705.
- (38) Vigier, F.; Coutanceau, C.; Hahn, F.; Belgsir, E. M.; Lamy, C. On the Mechanism of Ethanol Electro-Oxidation on Pt and PtSn Catalysts: Electrochemical and in Situ IR Reflectance Spectroscopy Studies. *J. Electroanal. Chem.* **2004**, *563*, 81–89.
- (39) Óvári, L.; Bugyi, L.; Majzik, Z.; Berkó, A.; Kiss, J. Surface Structure and Composition of Au–Rh Bimetallic Nanoclusters on TiO₂ (110): A LEIS and STM Study. *J. Phys. Chem. C* **2008**, *112*, 18011–18016.
- (40) Christensen, A.; Ruban, A. V.; Stoltze, P.; Jacobsen, K. W.; Skriver, H. L.; Nørskov, J. K.; Besenbacher, F. Phase Diagrams for Surface Alloys. *Phys. Rev. B: Condens. Matter Mater. Phys.* **1997**, *56*, 5822–5834.